Supporting Information

Atomic Modulation of Na^+ Transport Channels to Enhance Rate and Cycling Performance of Tunnel-Type Sodium Manganese Oxides

Chen Xu,[a] Qinghua Yi,[a] Kaibin Feng,[a] Jie Lai,[a] Zhihao Lin,[a] Yuanhao Zheng,[b] Xiao Yan,[b] Xi Chen,[c] Chenchen Wang*[a] and Zhe Hu*[a]

[a] Guangdong Provincial Key Laboratory of New Energy Materials Service Safety, College of Materials Science and Engineering, Shenzhen University, Shenzhen, Guangdong 518055, China.

[b] Institute of Technology for Future Industry, Shenzhen University of Information Technology, Shenzhen, Guangdong 518172, China.

[c] Department of Physics, School of Mathematics and Physics, Xi'an Jiaotong-Liverpool University, 111 Ren'ai Road, Suzhou Industrial Park, Suzhou 215123, P.R. China.

Experimental Section

Materials Synthesis: The pristine NMO, single-doped NMO-C0.5, NMO-C1, NMO-C2, NMO-C3, NMO-T5, NMO-T10, NMO-T15 and co-doped NMO-C0.5T10, NMO-C1T10, NMO-C2T10, NMO-C3T10 materials were synthesized via a high-temperature solid-state method. In accordance with the given chemical formula, stoichiometric amounts of Na_2CO_3 (with 5 wt% excess of sodium, 99%, Aladdin), $MnCO_3$ (99.95%, Aladdin), CuO (99%, Aladdin) and TiO_2 (99.99%, Aladdin) were thoroughly mixed and grounded for half an hour with mortar and pestle. The powder was pelleted and heated at 900℃ for 15h in a muffle furnace, then cooled to room temperature naturally.

Materials Characterizations: XRD patterns were obtained using a Rigaku SmartLabSE X-ray diffractometer (Cu Kα, λ = 1.54056 Å) in the 2θ range of 5°-80°. The obtained XRD patterns were subjected to Rietveld refinement analysis using the GSASII program.[40] *In-situ* XRD measurements were carried out using a custom designed *in-situ* battery holder, employing beryllium metal as the X-ray entrance window. The measurements were conducted at a fixed current density of 24 mA g^{-1} within the voltage range of 2.0-4.0 V. The Mn K-edge XAFS measurements were conducted at the XAFS spectroscopy (easy-XAFS) facility in transmission mode. The XAFS spectra were subsequently analyzed using the ATHENA software package.[41] The elemental stoichiometry in each sample was determined by ICAP 7000 SERIES inductively coupled plasma emission spec-trometry (ICP-OES). The morphology of samples was analyzed utilizing scanning electron microscopy (SEM, Thermo APREO S), coupled with EDS for elemental characterization, employing an operating voltage of 10 kV. HRTEM images were acquired using JEOL F200 operated. XPS measurements were carried out by using a Thermo Fisher ESCALAB 250xi system.

Electrochemical Measurements: The cathode electrodes were prepared by dispersing active materials into N-methyl-2-pyrrolidinone (NMP) with Super P and polyvinylidenefluoride (PVDF) in an 80:10:10 wt.% ratio and then coated on an aluminum foil with mass loading of 1-2 mg cm^{-2}. The electrodes were oven-dried at 100 °C under vacuum for 12 h. For all electrochemical measurements, 1M $NaClO_4$ in

ethylene carbonate (EC) and diethyl carbonate (DEC) (v/v = 1:1) solution was used as the electrolyte, and glass fiber was used as the separator. The materials were assembled in a coin cell (LIR-2032) with metallic sodium as both counter electrode and anode. For full-cell assembly, NMO-C1T10 and hard carbon (HC) were employed as the cathode and anode, respectively. The active mass ratio between the anode and cathode was carefully set at approximately 1:2.9 to balance capacity, and cycling tests were conducted within a fixed voltage window of 2.0-4.0 V. CV and EIS measurements were carried out on a CHI660E electrochemical workstation. All the EIS tests were conducted over a frequency range from 10^5 to 0.01 Hz. Galvanostatic charge-discharge tests were performed by using a Neware testing system at different conditions. For the *ex-situ* characterizations, the electrodes were collected by disassembling the electrochemical cells inside an Ar-filled glovebox and then washed three times with dimethyl carbonate (DMC).

Na^+ diffusion analysis: The chemical diffusion coefficients (D) of Na^+ in NMO and NMO-C1T10 were then evaluated by applying the Randles-Sevcik equation,[38,39]

$$I_p=2.69\times10^5 n^{\frac{3}{2}} A D^{\frac{1}{2}} v^{\frac{1}{2}} C_0 \quad (1)$$

where n is the electron transfer number during the redox reaction, A is the area of electrodes, v is the scan rate and C_0 is the Na^+ concentration in the lattice.

To qualitatively identify the charge storage mechanism, we first analyzed the relationship between Ip and v using the power-law equation:

$$I=av^b \quad (2)$$

By taking the logarithm of both sides, we obtained the linear transformation:

$$\lg(I_p)=b\cdot\lg(v)+\lg(a) \quad (3)$$

In this equation, the b-value (the slope) is a key indicator of the kinetic characteristics:

b = 0.5 indicates a pure diffusion-controlled (battery-type) process;

b = 1.0 represents a pure surface-controlled (capacitive) process;

$0.5 < b < 1.0$ signifies a mixed mechanism involving pseudocapacitance.

Our calculations show that the b-values for NMO and NMO-C1T10 are 0.8732 and 0.9356 (Fig. S22), respectively. These values, significantly higher than 0.5, demonstrate that pseudocapacitive contribution plays a substantial role in the electrochemical reaction, particularly for the modified NMO-C1T10.

According to Dunn's method, the total current at a fixed potential (V) can be expressed as the sum of two contributions:

$$I(V)=k_1v+k_2v^{1/2} \quad (4)$$

Where k_1v represents the capacitive current and $k_2v^{1/2}$ represents the diffusion-controlled current. When plotting I_p vs. (letting $x=v^{1/2}$), the equation becomes:

$$I_p= k_1x^2+k_2x \quad (5)$$

From a mathematical perspective, this is a quadratic relationship rather than a linear one. Within the experimental scan rate range (0.1 to 0.7 mV/s), the k_1x^2 term (pseudocapacitance) causes the I_p curve to deviate upwards. When we apply a linear fit to this slightly curved data, the resulting regression line inevitably exhibits a positive Y-intercept and does not pass through the origin.

Theoretical calculations: All calculations were carried out by using the Vienna Ab-initio Simulation Package (VASP) based on the density functional theory.[1] The projector-augmented wave was used for electron ion interactions.[2,3] Generalized gradient approximation with the Perdew–Burke–Ernzerhof functional was used to evaluate the exchange-correlation energy.[3] A plane-wave basis set was used with an energy cutoff of 520 eV. A 11 × 4 × 1 gamma-centered k-point grid was chosen. The climbing image nudged elastic band (CI-NEB) method was used to calculate the Na^+ diffusion barrier. The energy convergence tolerance was set to below 1×10^{-5} eV for atomic position relaxation and 1×10^{-8} eV. Atomic positions were fully optimized until the remaining force converged less than 0.02 eV $Å^{-1}$.

1. G. Kresse, J. Furthmüller, Comput. Mater. Sci. 1996, 6, 15.
2. P. E. Blöchl, Phys. Rev. B 1994, 50, 17953.
3. G. Kresse, D. Joubert, Phys. Rev. B 1999, 59, 1758.
4. J. P. Perdew, K. Burke, M. Ernzerhof, Phys. Rev. Lett. 1996, 77, 3865.

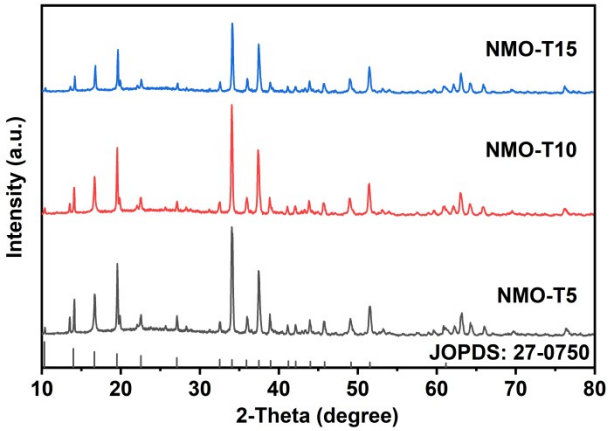

Fig. S1. XRD patterns of NMO-T5, NMO-T10 and NMO-T15.

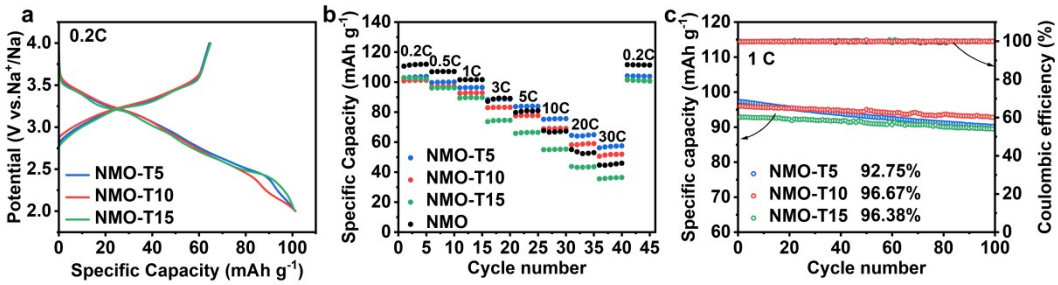

Fig. S2. A comparison of the electrochemical performance for NMO-T5, NMO-T10, and NMO-T15, showing: (a) charge-discharge curves at 0.2C (24 mA g^{-1}), (b) rate capability, and (c) cycle life at 1C for 100 cycles.

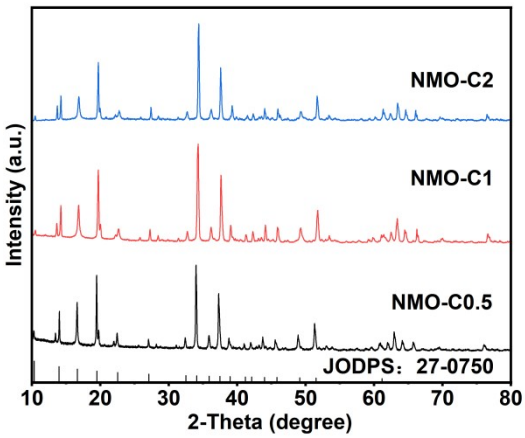

Fig. S3. XRD patterns of NMO-C0.5, NMO-C1 and NMO-C2.

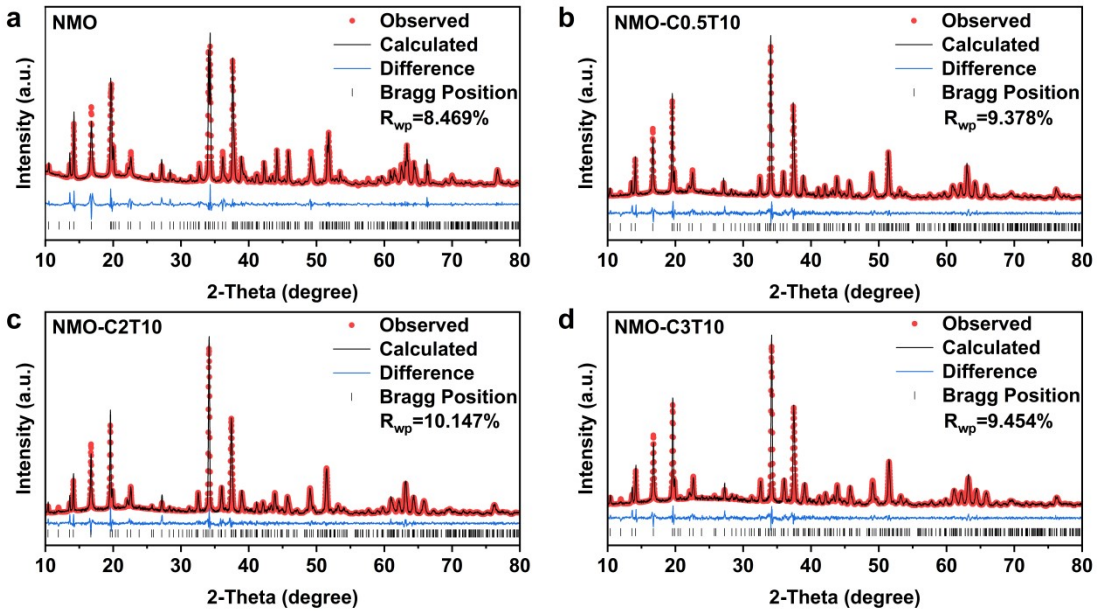

Fig. S4. XRD patterns and Rietveld refinement results of (a) NMO, (b) NMO-C0.5T10, (c) NMO-C2T10 and (d) NMO-C3T10.

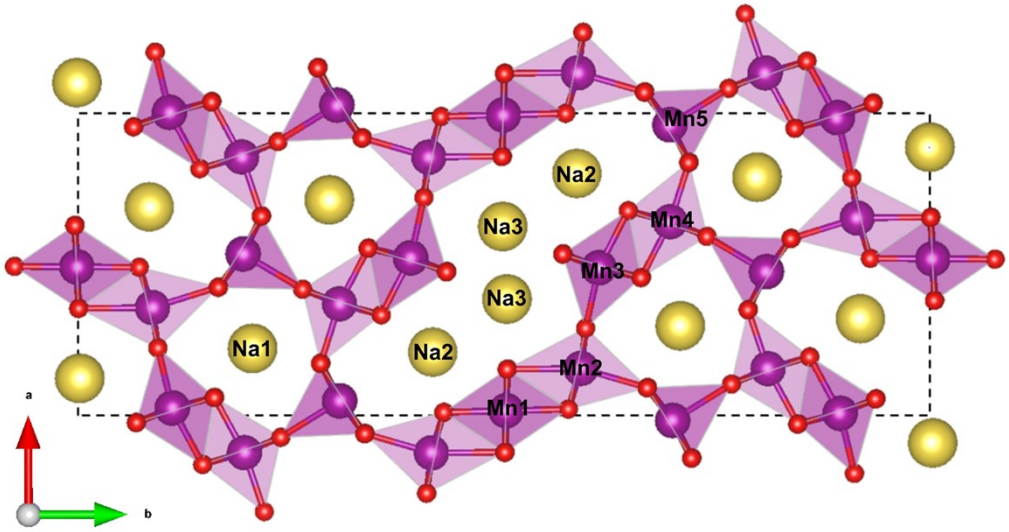

Fig. S5. The crystal structure of NMO.

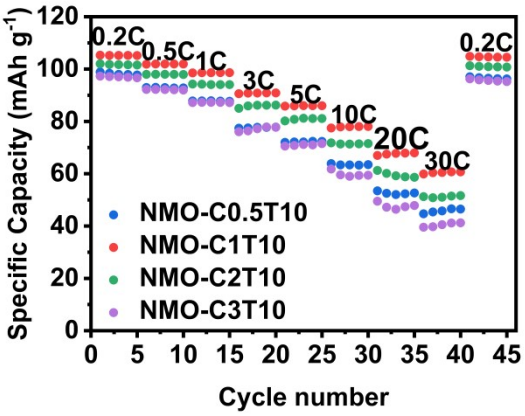

Fig. S6. Rate performances of the NMO-C0.5T10, NMO-C1T10, NMO-C2T10 and NMO-C3T10 cathodes.

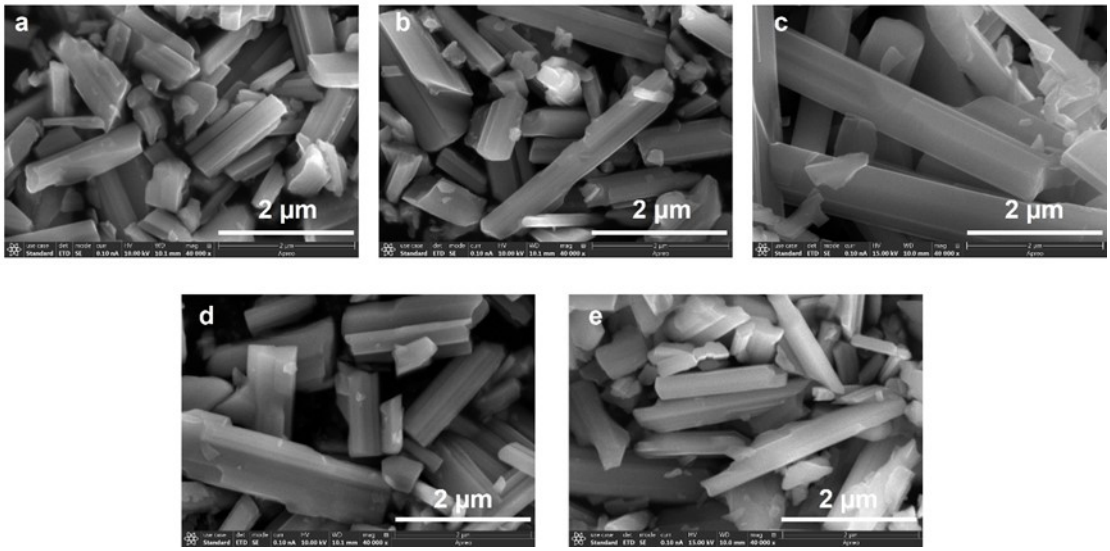

Fig. S7. SEM images of the (a) NMO, (b) NMO-C0.5T10, (c) NMO-C1T10, (d) NMO-C2T10 and (e) NMO-C3T10.

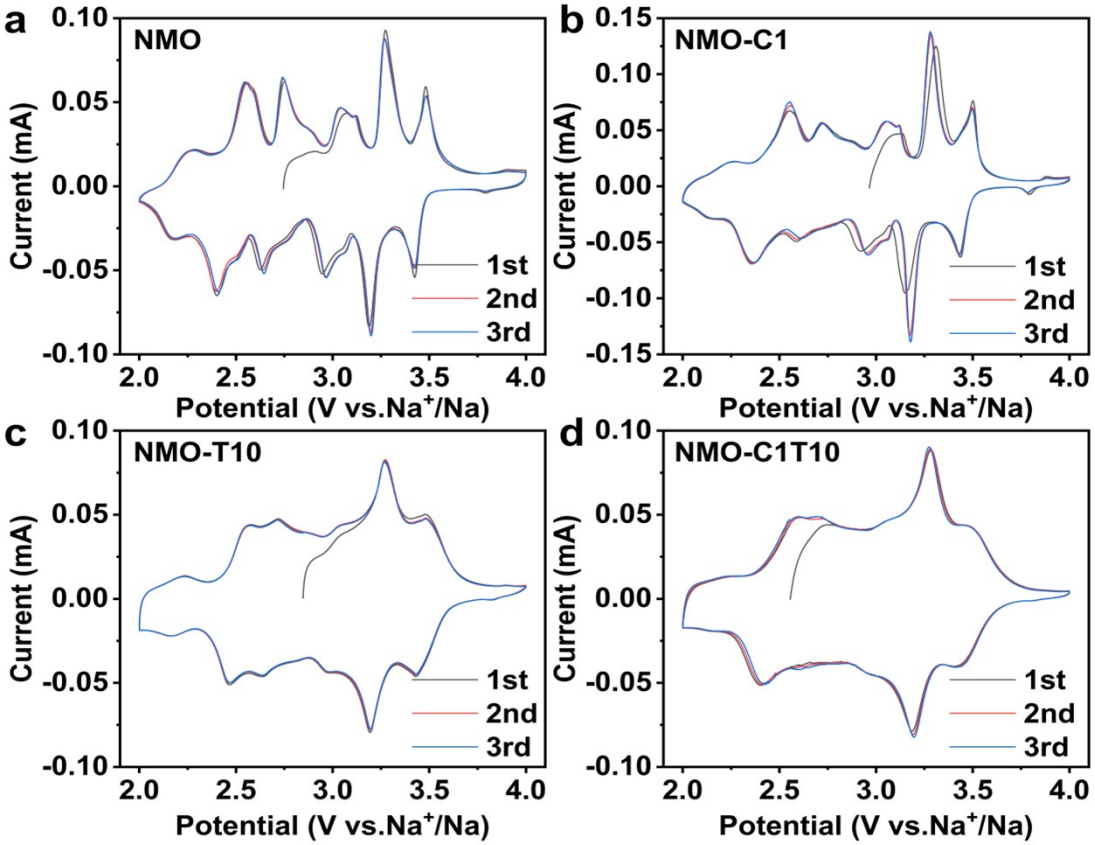

Fig. S8. CV curves of (a) NMO, (b) NMO-C1, (c) NMO-T10, (d) NMO-C1T10 electrode for the first three cycles between 2.0 and 4.0 V.

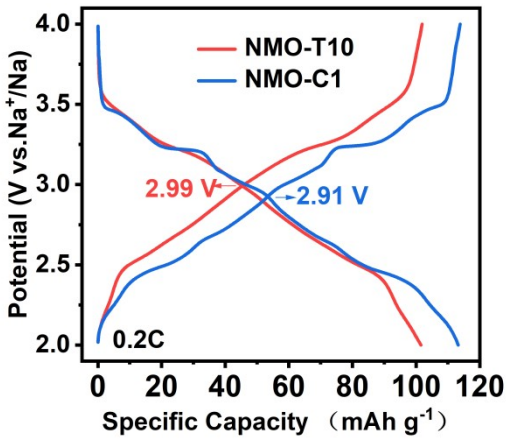

Fig. S9. Galvanostatic charge/discharge profiles of the NMO-T10 and NMO-C1 cathodes cycled between 2.0 and 4.0 V for the 2nd cycle at a current rate of 0.2C (24 mA g^{-1}).

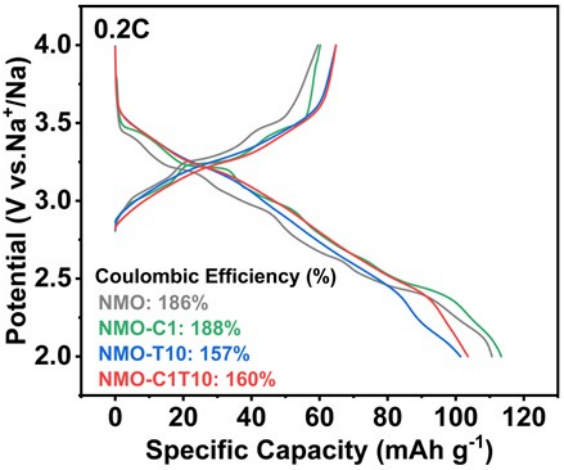

Fig. S10. Initial charge-discharge profiles and corresponding initial Coulombic efficiency (ICE) values of NMO, NMO-C1, NMO-T10, and NMO-C1T10 materials at a rate of 0.2C (24 mA g^{-1}).

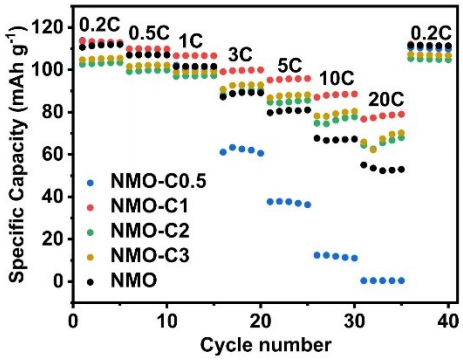

Fig. S11. Rate performances of the NMO, NMO-C1, NMO-C2, and NMO-C3 cathodes.

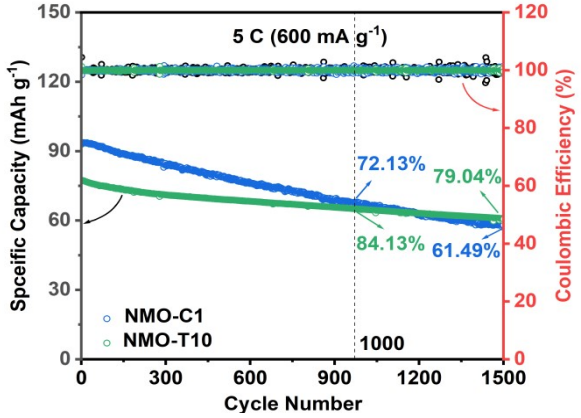

Fig. S12. Cycle performances of the NMO and NMO-C1T10 cathodes at 5C.

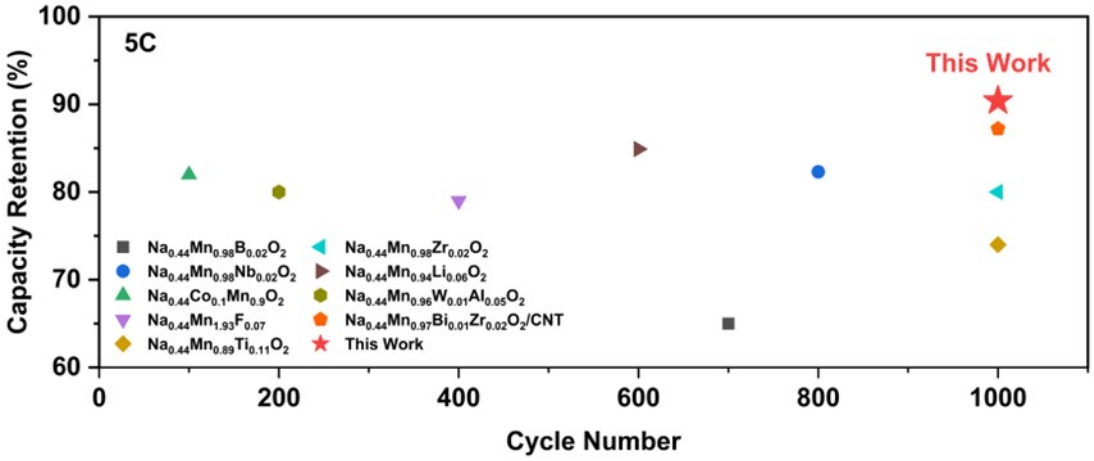

Fig. S13. High-rate long-cycle performance comparison of the Cu/Ti co-doped tunnel-type $Na_{0.44}MnO_2$ cathode developed in this work with other reported modified $Na_{0.44}MnO_2$-based cathodes at 5C.

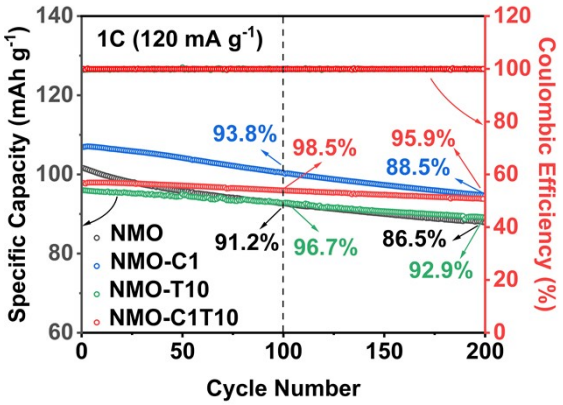

Fig. S14. The cycling performance of NMO, NMO-C1, NMO-C1T10, and NMO-T10 cathodes at 1C for 200 cycles.

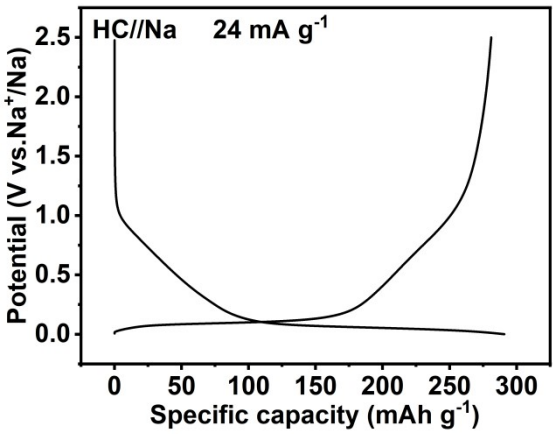

Fig. S15. The typical first discharge and charge profiles of hard carbon anode at 0.1C.

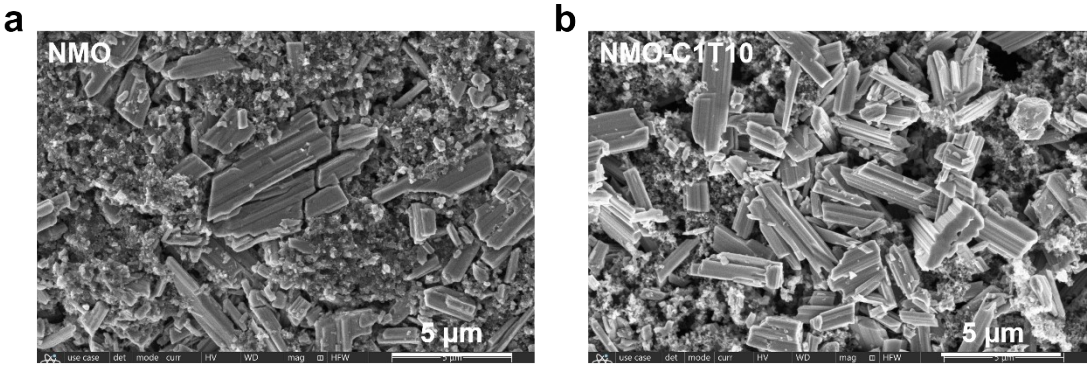

Fig. S16. SEM images of (a) NMO and (b) NMO-C1T10 cathodes after 200 cycles at 5 C (600 mA g^{-1})

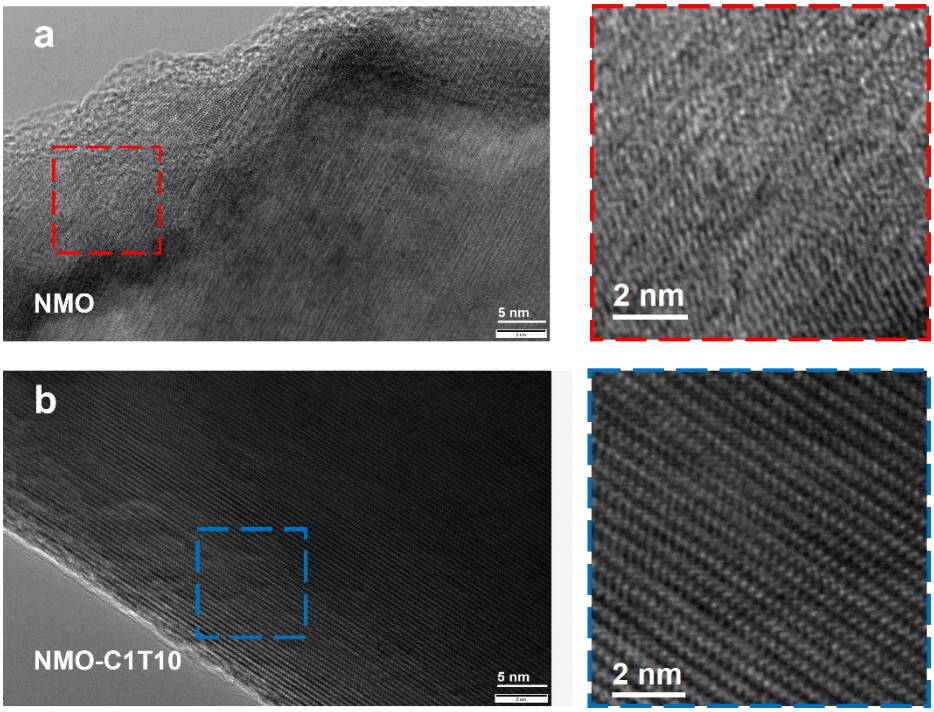

Fig. S17. TEM images of (a) NMO and (b) NMO-C1T10 cathodes after 200 cycles at 5 C (600 mA g^{-1})

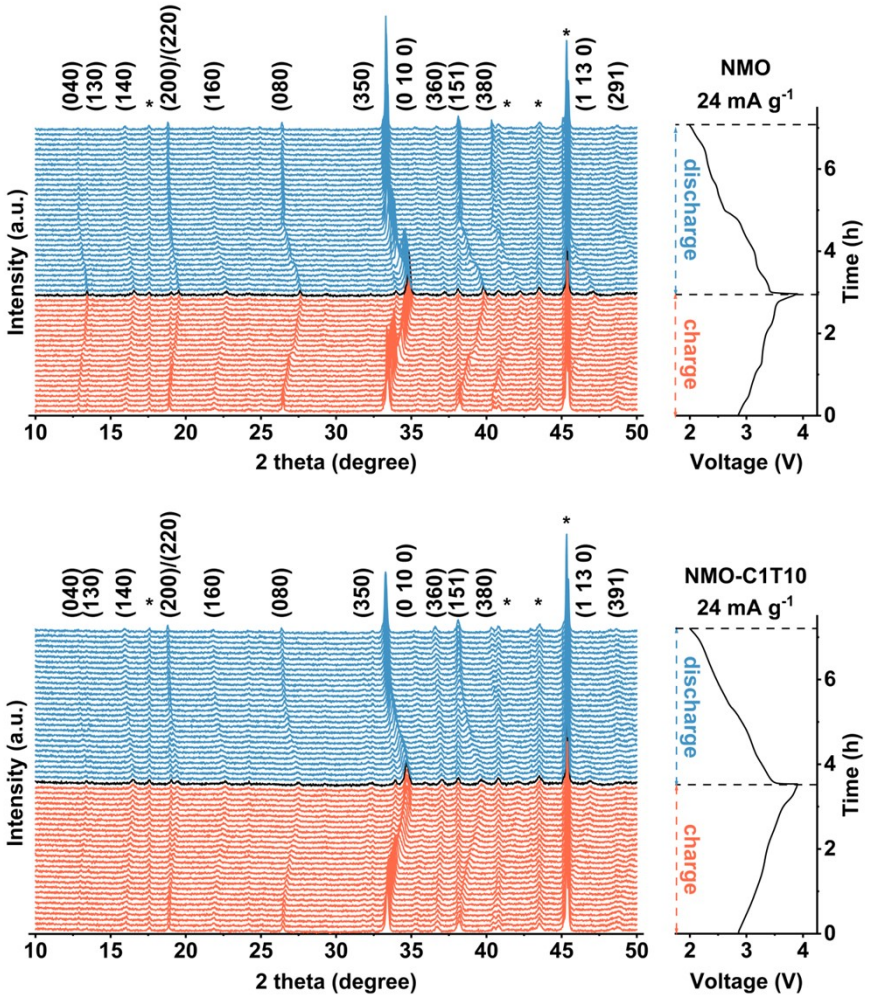

Fig. S18. *In-situ* XRD of (a) NMO and (b) NMO-C1T10.

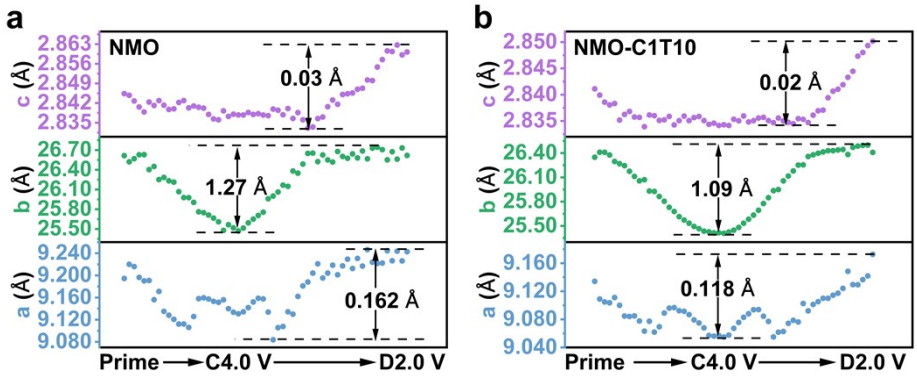

Fig. S19. Structural evolution of the cathode materials during the first charge-discharge cycle. Lattice parameters a, b and c obtained from Rietveld refinement of *in-situ* XRD patterns for (a) NMO and (b) NMO-C1T10.

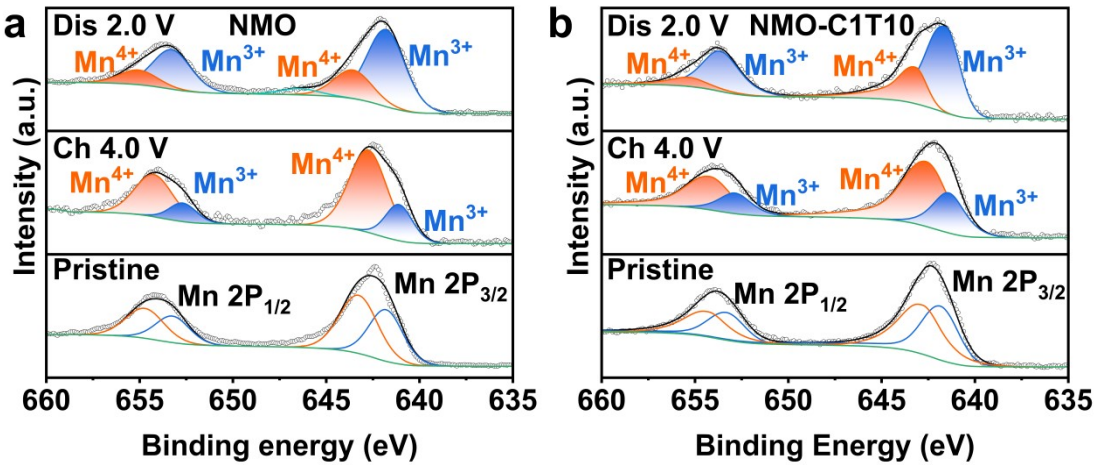

Fig. S20. Mn 2p XPS of (a) NMO and (b) NMO-C1T10 at pristine, charged and discharged state.

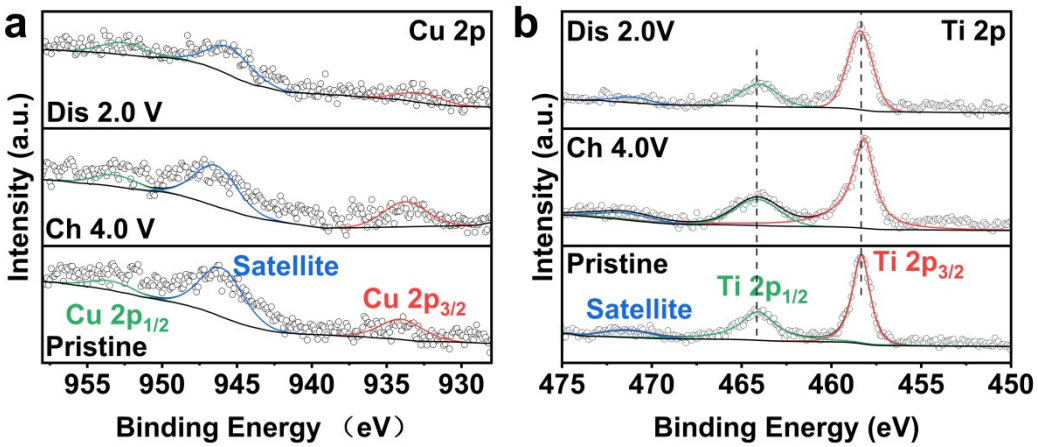

Fig. S21. (a) Cu 2p and (b) Ti 2p XPS of NMO-C1T10 at pristine, charged and discharged state.

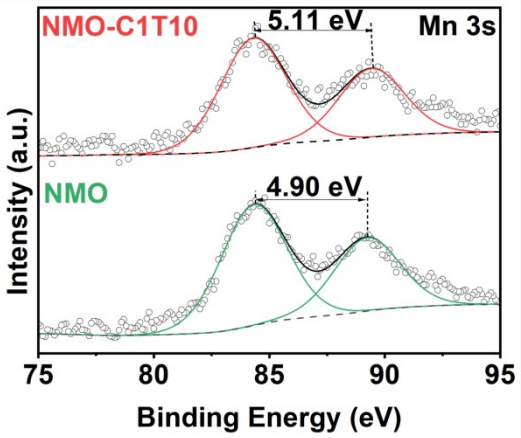

Fig. S22. XPS survey spectra of Mn 3s for NMO and NMO-C1T10 sample.

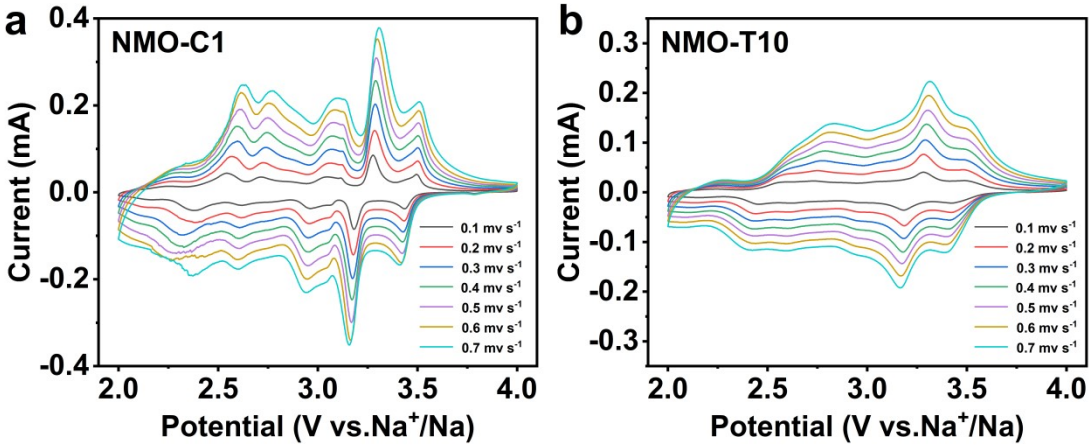

Fig. S23. CV curves of (a) NMO-C1 and (b) NMO-T10 cathodes at various scan rates (0.1, 0.2, 0.3, 0.4, 0.5, 0.6 and 0.7 mV s^{-1}).

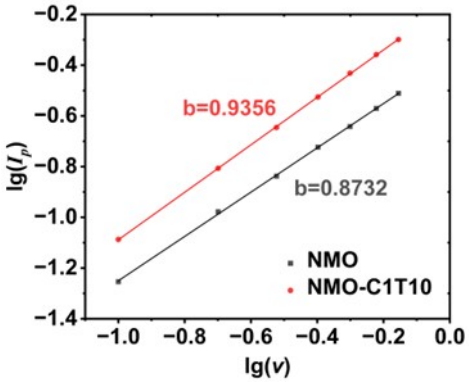

Fig. S24. Linear relationship between the logarithm of peak current lg(I_p) and the logarithm of scan rate lg(v).

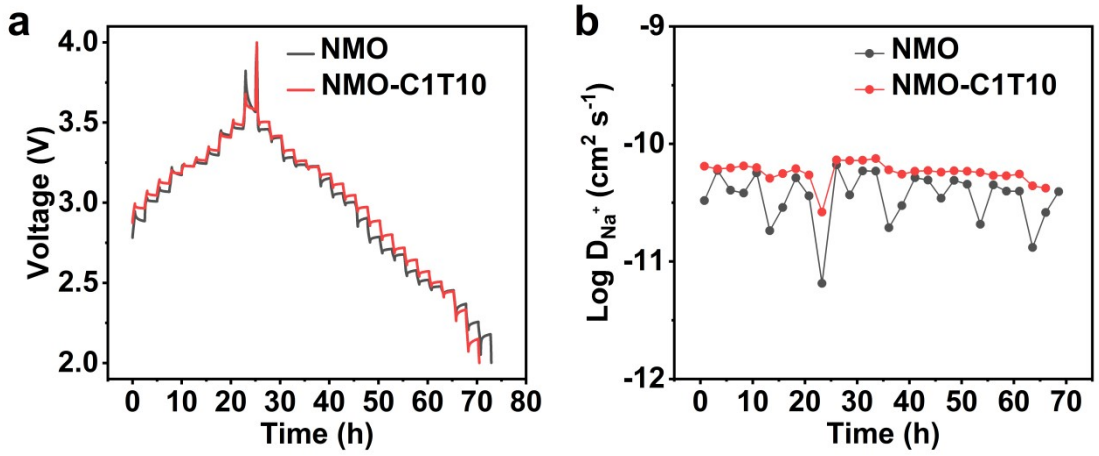

Fig. S25. (a) GITT curves of the NMO and NMO-C1T10 cathodes. (b) Calculated Na^+ diffusion coefficient of NMO and NMO-C1T10.

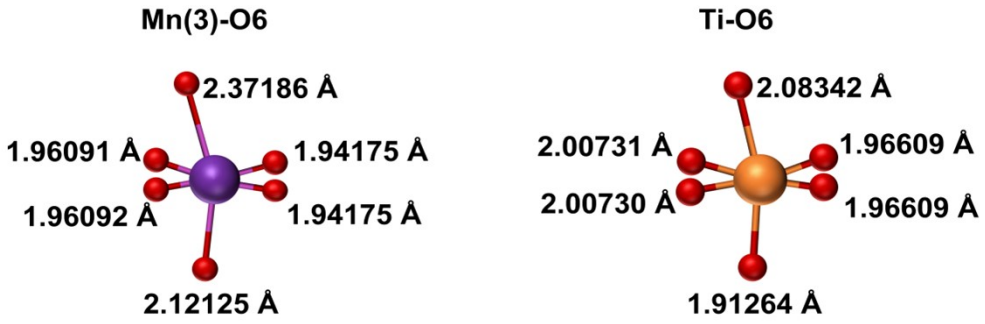

Fig. S26. Bond lengths of the Mn(3)-O6 and Ti-O6 coordination environments after structural optimization.

Fig. S27. Bond lengths of the Mn(5)-O5 and Cu-O5 coordination environments after structural optimization.

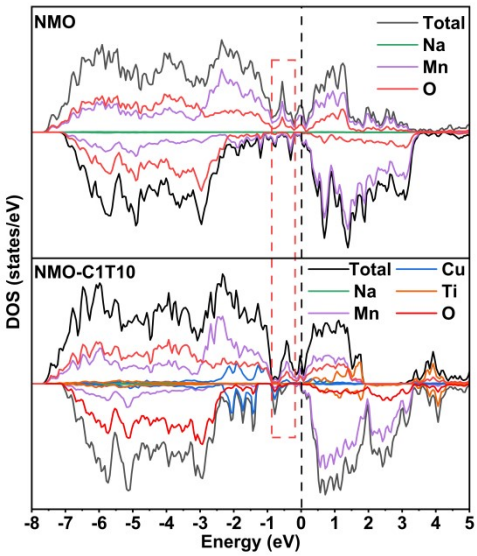

Fig. S28. Density of States (DOS) for NMO and NMO-C1T10 structures.

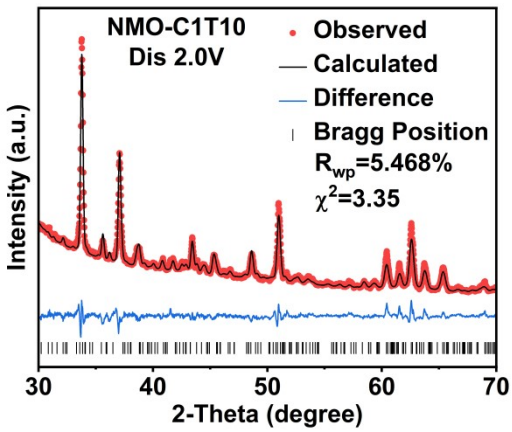

Fig. S29. XRD patterns and Rietveld refinement results of the NMO-C1T10 cathode discharged to 2.0V.

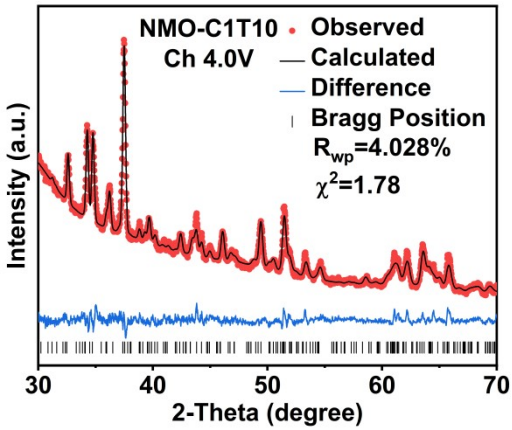

Fig. S30. XRD patterns and Rietveld refinement results of the NMO-C1T10 cathode charged to 4.0V.

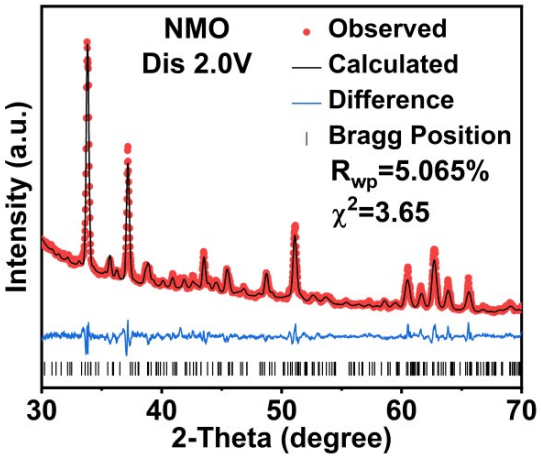

Fig. S31. XRD patterns and Rietveld refinement results of the NMO cathode discharged to 2.0V.

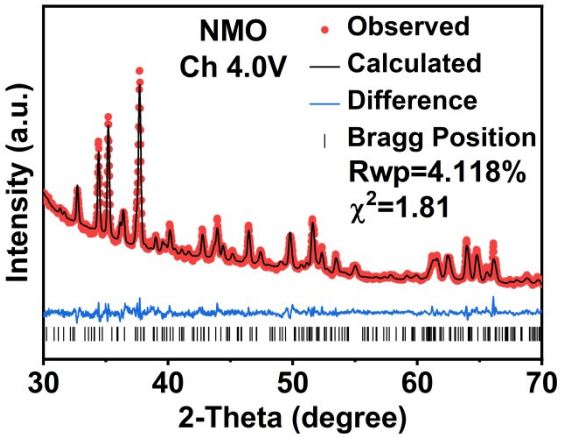

Fig. S32. XRD patterns and Rietveld refinement results of the NMO cathode charged to 4.0V.

Table S1. Refined crystallographic parameters of NMO-C1T10 by Rietveld analysis.

$Na_{0.44}Mn_{0.89}Cu_{0.01}Ti_{0.1}O_2$. Space group *Pbam*, a = 9.14519 Å, b = 26.43377 Å, c = 2.84315 Å, α = β = γ = 90°, V = 687.308 Å^3, R_{wp} = 5.103%, χ^2 = 1.41.

Atom	x	y	z	site	Occupation
Na1	0.21870	0.20364	0.00000	*4g*	0.9000
Na2	0.20051	0.41546	0.50000	*4h*	0.4300
Na3	0.12098	0.00396	0.00000	*4g*	0.6500
Mn1	0.00000	0.50000	0.00000	*2c*	1.0000
Mn2	0.36079	0.08878	0.50000	*4h*	0.0000
Mn3	0.01698	0.11037	0.00000	*4g*	0.5500
Mn4	0.36704	0.30608	0.50000	*4h*	1.0000
Mn5	0.04099	0.30538	0.00000	*4g*	0.9550
O1	0.35718	0.00227	0.50000	*4h*	1.0000
O2	0.22319	0.09278	0.00000	*4g*	1.0000
O3	0.04598	0.16049	0.50000	*4h*	1.0000
O4	0.43084	0.16657	0.50000	*4h*	1.0000
O5	0.16249	0.28239	0.50000	*4h*	1.0000
O6	0.41749	0.26527	0.00000	*4g*	1.0000
O7	0.32442	0.35512	0.00000	*4g*	1.0000
O8	0.50185	0.07275	0.00000	*4g*	1.0000
O9	0.47180	0.43200	0.50000	*4h*	1.0000
Cu	0.04099	0.30538	0.00000	*4h*	0.0450
Ti	0.01698	0.11037	0.00000	*4g*	0.4500

Table S2. Refined crystallographic parameters of NMO by Rietveld analysis.

$Na_{0.44}MnO_2$. Space group *Pbam*, a = 9.10247 Å, b = 26.45419 Å, c = 2.82761 Å, $\alpha = \beta = \gamma = 90°$, $V = 680.885$ Å^3, $R_{wp} = 8.469\%$, $\chi^2 = 3.84$.

Atom	x	y	z	site	Occupation
Na1	0.21850	0.20430	0.00000	*4g*	0.9000
Na2	0.20030	0.41480	0.50000	*4h*	0.4300
Na3	0.12270	0.00210	0.00000	*4g*	0.6500
Mn1	0.00000	0.50000	0.00000	*2c*	1.0000
Mn2	0.35970	0.08780	0.50000	*4h*	1.0000
Mn3	0.01960	0.10990	0.00000	*4g*	1.0000
Mn4	0.36640	0.30630	0.50000	*4h*	1.0000
Mn5	0.03840	0.30560	0.00000	*4g*	1.0000
O1	0.35960	0.00180	0.50000	*4h*	1.0000
O2	0.22320	0.09380	0.00000	*4g*	1.0000
O3	0.05390	0.15930	0.50000	*4h*	1.0000
O4	0.42690	0.16520	0.50000	*4h*	1.0000
O5	0.16610	0.28380	0.50000	*4h*	1.0000
O6	0.41730	0.26350	0.00000	*4g*	1.0000
O7	0.32790	0.35520	0.00000	*4g*	1.0000
O8	0.49660	0.07280	0.00000	*4g*	1.0000
O9	0.47180	0.43200	0.50000	*4h*	1.0000

Table S3. Stoichiometry of NMO-C1T10 from ICP test.

Element	Content (mg/L)	Mol ratio
Na	2.0930	0.4444
Mn	9.8430	0.8746
Cu	0.1490	0.0114
Ti	1.1170	0.1139

Table S4. Comparison of the ionic radii and Coordination environment with oxygen between the ions involved in this work.

	Ionic Radius(Å)	**TM-O5**	**TM-O6**
Mn^{3+}	0.65	✔	✔
Mn^{4+}	0.53	×	✔
Cu^{+}	0.96	×	×
Cu^{2+}	0.72	✔	✔
Ti^{2+}	0.90	×	×
Ti^{3+}	0.76	×	✔
Ti^{4+}	0.68	✔	✔

Table S5. Crystallographic parameters of the NMO-C1T10 cathode discharged to 2.0V refined by Rietveld analysis.

$Na_{0.44}Mn_{0.89}Cu_{0.01}Ti_{0.1}O_2$. Space group *Pbam*, a = 9.20126 Å, b = 26.50987 Å, c = 2.85488 Å, $\alpha = \beta = \gamma = 90°$, $V = 696.374$ Å^3, $R_{wp} = 5.468\%$, $\chi^2 = 3.35$.

Atom	x	y	z	site	Occupation
Na1	0.22582	0.20168	0.00000	*4g*	0.9000
Na2	0.14979	0.40321	0.50000	*4h*	0.6426
Na3	0.20007	0.00469	0.00000	*4g*	0.9319
Mn1	0.00000	0.50000	0.00000	*2c*	1.0000
Mn2	0.35803	0.08998	0.50000	*4h*	0.0000
Mn3	0.00259	0.10876	0.00000	*4g*	0.5500
Mn4	0.34987	0.30745	0.50000	*4h*	1.0000
Mn5	0.02845	0.30419	0.00000	*4g*	0.9550
O1	0.35144	0.00191	0.50000	*4h*	1.0000
O2	0.22942	0.08620	0.00000	*4g*	1.0000
O3	0.05063	0.16186	0.50000	*4h*	1.0000
O4	0.41827	0.16888	0.50000	*4h*	1.0000
O5	0.14900	0.27167	0.50000	*4h*	1.0000
O6	0.45237	0.27044	0.00000	*4g*	1.0000
O7	0.34446	0.35334	0.00000	*4g*	1.0000
O8	0.48849	0.07381	0.00000	*4g*	1.0000
O9	0.46875	0.43462	0.50000	*4h*	1.0000
Cu	0.25688	0.23835	0.00000	*4h*	0.0450
Ti	0.01075	0.10905	0.00000	*4g*	0.4500

Table S6. Crystallographic parameters of the NMO-C1T10 cathode charged to 4.0V refined by Rietveld analysis.

$Na_{0.44}Mn_{0.89}Cu_{0.01}Ti_{0.1}O_2$. Space group: *Pbam*, a = 9.10961 Å, b = 25.80805 Å, c = 2.83811 Å, α = β = γ = 90°, V = 667.244 Å^3, R_{wp} = 4.102%, χ^2 = 1.78.

Atom	x	y	z	site	Occupation
Na1	0.22349	0.21019	0.00000	*4g*	0.8946
Na2	0.18337	0.39314	0.50000	*4h*	0.1780
Na3	0.12270	0.00210	0.00000	*4g*	0.0321
Mn1	0.00000	0.50000	0.00000	*2c*	1.0000
Mn2	0.37726	0.09017	0.50000	*4h*	0.0000
Mn3	0.01500	0.10904	0.00000	*4g*	0.5500
Mn4	0.37507	0.30887	0.50000	*4h*	1.0000
Mn5	0.04681	0.30746	0.00000	*4g*	0.9550
O1	0.37126	0.01114	0.50000	*4h*	1.0000
O2	0.23549	0.10478	0.00000	*4g*	1.0000
O3	0.06338	0.16302	0.50000	*4h*	1.0000
O4	0.42359	0.17333	0.50000	*4h*	1.0000
O5	0.17171	0.28805	0.50000	*4h*	1.0000
O6	0.41833	0.26431	0.00000	*4g*	1.0000
O7	0.34170	0.35459	0.00000	*4g*	1.0000
O8	0.49709	0.07297	0.00000	*4g*	1.0000
O9	0.47678	0.43387	0.50000	*4h*	1.0000
Cu	0.07316	0.32183	0.00000	*4h*	0.0450
Ti	0.03845	0.11294	0.00000	*4g*	0.4500

Table S7. Crystallographic parameters of the NMO cathode discharged to 2.0V refined by Rietveld analysis.

$Na_{0.44}MnO_2$. Space group *Pbam*, a = 9.19535 Å, b = 26.46181 Å, c = 2.84544 Å, α = β = γ = 90°, V = 692.368Å^3, R_{wp} = 5.605%, χ^2 = 3.65.

Atom	x	y	z	site	Occupation
Na1	0.21684	0.19893	0.00000	*4g*	0.9000
Na2	0.14937	0.40173	0.50000	*4h*	0.6234
Na3	0.15129	0.00711	0.00000	*4g*	0.9053
Mn1	0.00000	0.50000	0.00000	*2c*	1.0000
Mn2	0.35065	0.09111	0.50000	*4h*	0.0000
Mn3	0.00317	0.10978	0.00000	*4g*	0.5500
Mn4	0.34394	0.30771	0.50000	*4h*	1.0000
Mn5	0.02449	0.30252	0.00000	*4g*	0.9550
O1	0.35964	0.00177	0.50000	*4h*	1.0000
O2	0.23131	0.08626	0.00000	*4g*	1.0000
O3	0.04605	0.16291	0.50000	*4h*	1.0000
O4	0.42550	0.16888	0.50000	*4h*	1.0000
O5	0.15393	0.27298	0.50000	*4h*	1.0000
O6	0.45512	0.27211	0.00000	*4g*	1.0000
O7	0.33795	0.35367	0.00000	*4g*	1.0000
O8	0.48681	0.07297	0.00000	*4g*	1.0000
O9	0.47450	0.43499	0.50000	*4h*	1.0000

Table S8. Crystallographic parameters of the NMO cathode charged to 4.0V refined by Rietveld analysis.

$Na_{0.44}MnO_2$. Space group *Pbam*, a = 9.09536 Å, b = 25.50541 Å, c = 2.82549 Å, α = β = γ = 90°, V = 655.459 Å^3, R_{wp} = 4.118%, χ^2 = 1.81.

Atom	x	y	z	site	Occupation
Na1	0.24834	0.20583	0.00000	*4g*	0.9000
Na2	0.36270	0.38649	0.50000	*4h*	0.2332
Na3	0.10632	0.00420	0.00000	*4g*	0.2328
Mn1	0.00000	0.50000	0.00000	*2c*	1.0000
Mn2	0.36701	0.09120	0.50000	*4h*	0.0000
Mn3	0.02558	0.11126	0.00000	*4g*	0.5500
Mn4	0.37195	0.30876	0.50000	*4h*	1.0000
Mn5	0.04590	0.30980	0.00000	*4g*	0.9550
O1	0.34626	0.01230	0.50000	*4h*	1.0000
O2	0.23631	0.09866	0.00000	*4g*	1.0000
O3	0.06458	0.17417	0.50000	*4h*	1.0000
O4	0.43067	0.18130	0.50000	*4h*	1.0000
O5	0.17093	0.29214	0.50000	*4h*	1.0000
O6	0.42164	0.27065	0.00000	*4g*	1.0000
O7	0.34391	0.34916	0.00000	*4g*	1.0000
O8	0.50951	0.07494	0.00000	*4g*	1.0000
O9	0.48502	0.43677	0.50000	*4h*	1.0000